Characterisation of Organic Thin Film Coatings on Automobile Steel Sheets by Photothermal Methods

Thomas ORTH, Salzgitter Mannesmann Forschung GmbH, Duisburg, Germany
Wilko FLÜGGE, Salzgitter Mannesmann Forschung GmbH, Salzgitter, Germany
Jürgen GIBKES, AG FestKörperSpektroskopie, Ruhr-Universität, Bochum, Germany

Abstract. In the nineties, the first generation of organic thin film coatings for corrosion protection of zinc-coated thin sheet steel have been introduced. The coating typically consists of a suspension of small zinc particles, embedded in a polymer matrix. In the scope of quality control, the characterisation of the resulting layer structure is of great interest, comprising not only a constant layer thickness and a local homogeneity of the coating, but also the depth distribution of the particles within the layer. Especially the latter parameter does have a direct influence on the spot weldability of the steel sheets.

The present work shows, how photothermal methods like modulated infrared radiometry and photoacoustics can be used for a successful depth profiling of the thin film coatings. The sample surface is periodically heated using an intensity-modulated laser beam, and a thermal wave is induced in the layer system. By variation of the modulation frequency of the laser beam, the thermal diffusion length and, as a consequence, the penetration depth of the thermal wave can be adjusted.

By a suitable evaluation of the amplitude and phase lag signals as a function of the modulation frequency, accurate depth profiling has been realized which can be used for a very reliable prediction of the welding properties of the product.

In the first investigations, artificial samples with well defined extreme distributions of the particles have been analyzed, and in a second step, an evaluation strategy has been developed for real production samples.

1. Introduction

One of the major challenges for European coil coating lines in the steel industry is the development of materials based on electro-galvanized steel covered by a thin weldable organic coating as corrosion protection primer on one or both sides. The thin organic films of about 2.5 - 4 µm thickness (1st generation) are applied directly after chemical chromate-free pre-treatment by roll coater on continuous coil lines. The coating consists of a suspension of small zinc particles, embedded in a polymer matrix (Figure 1).

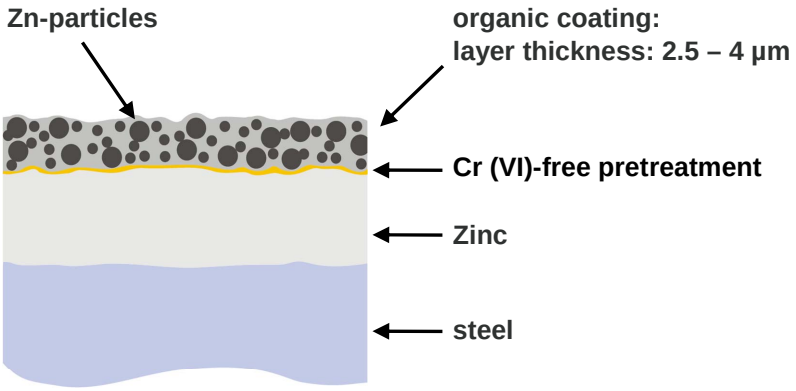

Figure 1. Principle of layer structure of a corrosion protection primer of the first generation

The mean size of the particles is about 2 µm. The particle size distribution exhibits a considerable variation, resulting in particle sizes from less than 1 µm to comparable with the layer thickness. Apart from corrosion protection, the primer also fulfils requirements concerning forming behaviour, paint adhesion, bonding, and weldability. These coatings have to protect car bodies reliably against corrosion, above all in poorly accessible flange sections, thus eliminating the need for waxing [1,2].

In the scope of quality control, the characterisation of the resulting layer structure is of great interest, comprising not only a constant layer thickness and local homogeneity of the coating, but also a good weldability of the steel coils. For this purpose, the coils are analysed with respect to the electrical resistance in a spot welding-like electrode configuration (Figure 2), and above certain resistance thresholds (2 mOhm according to Daimler-Chrysler specification), the coil will be submitted to additional tests. Unfortunately, this method does not directly correlate with the causes of good or poor weldability which probably is governed by the distribution of the particles within the layer system, and any deviation from the ideal homogeneous particle distribution profile will probably lead to changes of the welding properties.

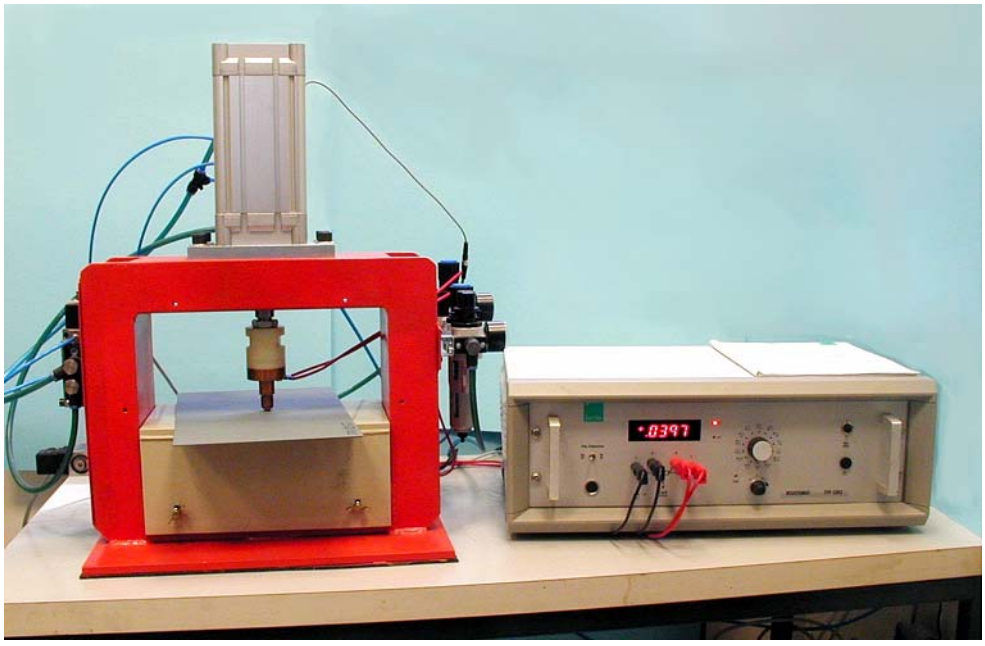

Figure 2. Laboratory system to measure the electrical resistance of spot-welded joints

Up to now, this particle distribution can only be measured by time consuming destructive methods such as Glow Discharge Optical Emission Spectroscopy (GDOES). For this reason, a fast non-destructive technique, which can be used parallel to the production process, is of great interest.

In the following, we will show how photothermal methods like modulated infrared radiometry and photoacoustics can be used for successful depth profiling studies of the thin film coatings on steel. In Sect. 2, the principles of photothermal measurements and the applied measuring system are briefly described. In Sect. 3 test samples with well defined extreme particle distributions are analysed, and in Sect. 4, an evaluation strategy is developed to distinguish between real production samples of good and bad welding properties, and the possibilities of an on-line quality control of the coating process is discussed.

2. Principles of Photothermal Characterization of Coatings – Measurement System

In photothermal characterization of coated solids, small periodical temperature oscillations, so-called thermal waves, are excited with the help of an intensity-modulated laser beam absorbed at the surface of the coating. At the interfaces between different layers, e.g. between coating and substrate, the thermal waves are partially reflected, and the resulting thermal wave is then measured at the surface. Excitation and propagation of thermal waves, which are governed by the heat diffusion equation, depend on the localization of the modulated heat sources, the effective thermal transport properties, and the thickness of different layers. The schematic of the measuring system used for this study is shown in Figure 3.

For the excitation of thermal waves, a Laser beam in the visible spectrum is used, with a beam power of about 1 W and a diameter of about 2 mm, intensity-modulated with the help of an acousto-optical modulator (Laser Components, LM 080). Modulated heating of the samples in the frequency interval between 0.03 Hz and 100 kHz takes place at the samples' front surface, where the modulated IR signal is detected with the help of a MCT detector (Judson-Infrared, JD15-D12) allowing a maximum detectable wavelength interval of 2 µm – 12µm.

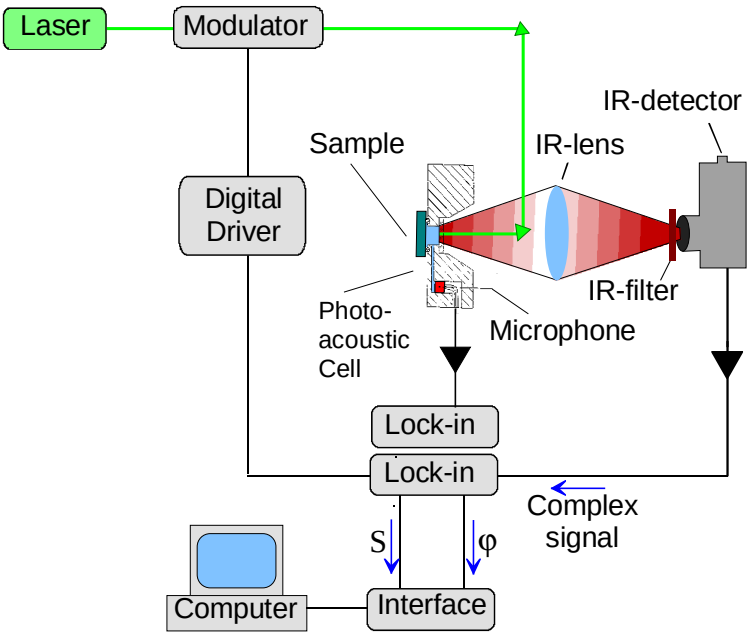

Figure 3. Schematic of the measurement device, enabling simultaneously IR radiometric and photoacoustic detection of thermal waves

Owing to the fact that the organic coatings are semi-transparent, both in the visible and in the IR spectral range, and that the semi-transparency varies with the distribution of the zinc particles, two detection techniques are applied simultaneously: Modulated IR radiometry and Photoacoustics. Photoacoustic detection, realized with the help of a gas microphone (Sennheiser KE4-211) inside a photoacoustic cell (Figure 3), is sensitive to the thermal properties and to the optical properties in the visible spectrum, while Modulated IR radiometry is sensitive to the thermal properties, to the optical properties in the visible spectrum, and to the IR optical properties. By combining photoacoustic detection and IR radiometry, the optical and IR optical properties can be distinguished [3]. To analyze the signals detected by the microphone and the MCT detector, two lock-in amplifiers are used, which are two-phase lock-in amplifiers (SR 830), enabling to measure both the thermal wave amplitude and the phase lag relative to the phase of the heating modulation.

Once the optical properties of the coatings have been analyzed in detail, only modulated IR radiometry will be applied in possible industrial on-line applications.

3. Measurements of Test Samples with Well Defined Zinc Particle Distributions

In the first investigations, specially prepared samples with well defined extreme distributions of the zinc particles have been analyzed, e.g. with top and bottom layers with and without zinc particles (compare Table 1).

Table 1. Layer structure of the semi-transparent coated steel sheet samples

Sample	Symbol in Fig.4-8	Layer structure	
A	■	3 µm varnish layer with homogeneous Zn particle distribution	
B	●	4 µm varnish layer without Zn particles	
C	♦	3 µm top layer with Zn particles	1 µm intermediate varnish layer
D	+	1 µm top layer with Zn particles	3 µm intermediate varnish layer
E	▲	3 µm top layer without Zn particles	1 µm intermediate layer with Zn particles
F	▼	1 µm top layer without Zn particles	3 µm intermediate layer with Zn particles

In Figure 4 the modulated IR amplitudes measured as a function of modulation frequency for several test samples of known layer structure are shown, in comparison with the signals measured for two homogeneous reference samples, namely a sample of opaque glassy carbon (Sigradur) and a sample of semi-transparent neutral density glass (Schott, NG1). In the range of intermediate modulation frequencies, 10 Hz < f < 20 kHz, the modulated IR amplitudes measured for glassy carbon (□) exhibit a modulation frequency dependence according to $f^{-1/2}$, as expected for opaque homogeneous semi-infinite solids of smooth surface, while the modulated IR amplitudes measured for neutral density glass (□) exhibit the modulation frequency dependence f^{-1}, expected for semi-transparent homogeneous solids.

In the limit of high modulation frequencies, f > 20 kHz, the modulated IR amplitudes of the homogeneous reference sample (□) show a slightly stronger decrease with increasing modulation frequency which is due to the frequency characteristics of the measurement system. Since this frequency characteristic affects all measured signals in the same way, it can be eliminated, when the signals of the coated steel sheet samples are interpreted in the calibrated form, with the signals of the homogeneous samples of glassy carbon used as reference for calibration (compare Sect. 3.1).

In comparison to the opaque homogeneous reference sample of glassy carbon (□), the modulated IR amplitudes measured for the samples A(■), C(♦), D(+), E(▲) and F(▼) exhibit a curved amplitude decrease with increasing modulation frequencies, clearly pointing towards a layer structure, while the sample B(●) exhibits a less curved decrease with

increasing modulation frequencies, which at high modulation frequencies is close to the behavior of the homogeneous semi-transparent neutral density glass reference sample (□).

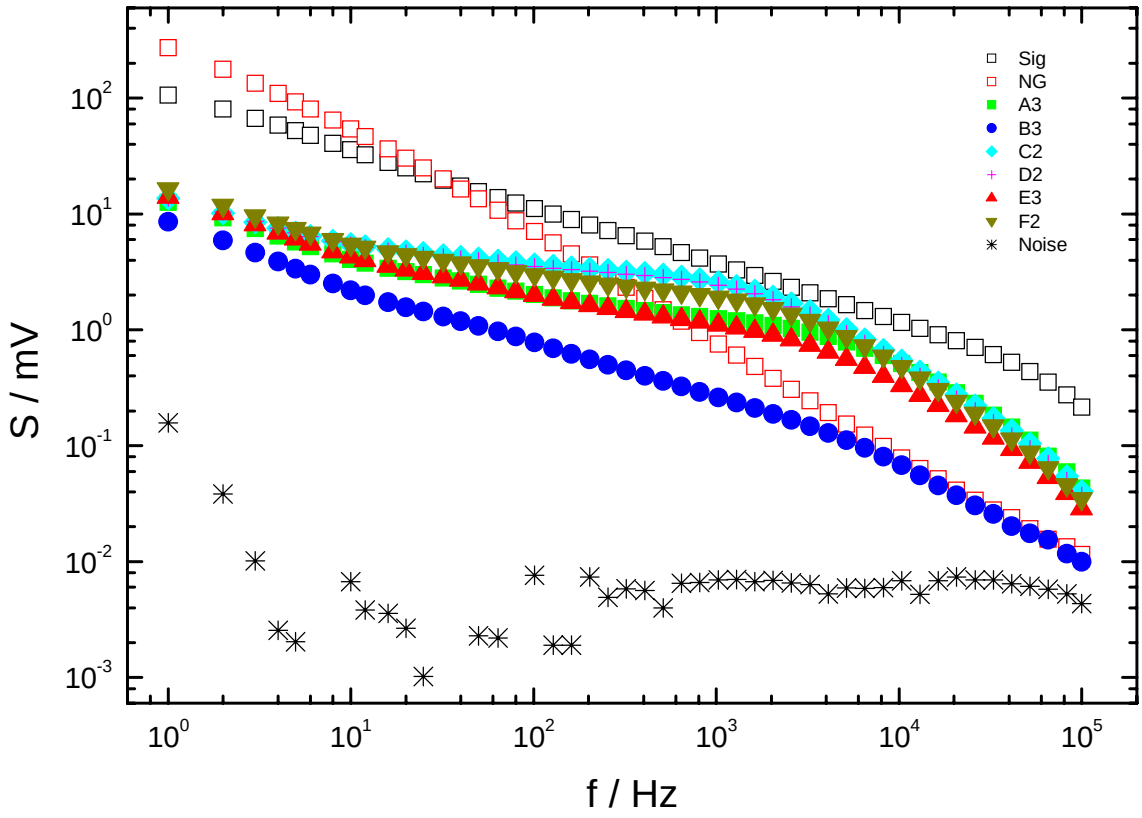

Figure 4. Modulated IR amplitudes measured as a function of the heating modulation frequency for coated steel sheet samples, in comparison with the noise signal (∗) and the reference signals measured for opaque homogeneous glassy carbon (Sigradur □) and semi-transparent neutral density glass (Schott NG1 □).

At higher modulation frequencies, above about 10 kHz, the modulated IR amplitudes of the other samples, A(■), C(♦), D(+), E(▲), and F(▼), also show this transition to the signals of the semi-transparent reference sample, due to the fact that all coatings are semi-transparent in the visible and/ or in the IR spectral range.

At first glance, it can already be stated here that the samples C(♦) and D(+) are very similar to each other (compare Table 1), and that the samples A(■) and E(▲) also seem to be similar to each other (Figure 4).

In Figure 4, the noise signals (∗) measured with the heating laser beam screened off are also presented: $1/f$ – noise in the range between 1 Hz and 100 Hz, and nearly constant IR background fluctuations at higher modulation frequencies [4]. In general, the modulated IR signals of the different coated samples are considerably above the IR background fluctuation limit and thus can be interpreted over the whole measured frequency interval.

In Figure 5 the modulated IR phases are shown, measured for the coated steel sheet test samples and the two reference samples. In the range of the intermediate modulation frequencies, 10 Hz < f < 4 kHz, the modulated IR phases (Fig 5) measured for the reference sample of glassy carbon (□) are close to 135°, showing a phase retardation of about - 45° relative to the phase of 180° of the modulated excitation. This phase lag of - 45° is characteristic for one-dimensional thermal wave propagation in an opaque homogeneous semi-infinite body. The modulated IR phases measured for the semi-transparent neutral density glass sample (□) are found between 120° and 90°.

In the range of low modulation frequencies, when the thermal diffusion lengths are comparable with or larger than the heating spot diameter,

$$\mu_{th} = \sqrt{\alpha/(\pi f)} \geq d_H \qquad (1)$$

three-dimensional thermal wave propagation becomes dominant and the modulated IR phases remain close to 180°, corresponding to a smaller phase retardation, $0 \geq \Delta\Phi > -45°$.

In the limit of high modulation frequencies, the modulated IR phases of the reference samples and of all coated steel sheet test samples show values considerably below 135°. This effect, which is also due to the frequency characteristics of the measuring system and which is common to all measured modulated IR phases can be eliminated when the calibrated modulated IR phases are considered (compare Sect. 3.1).

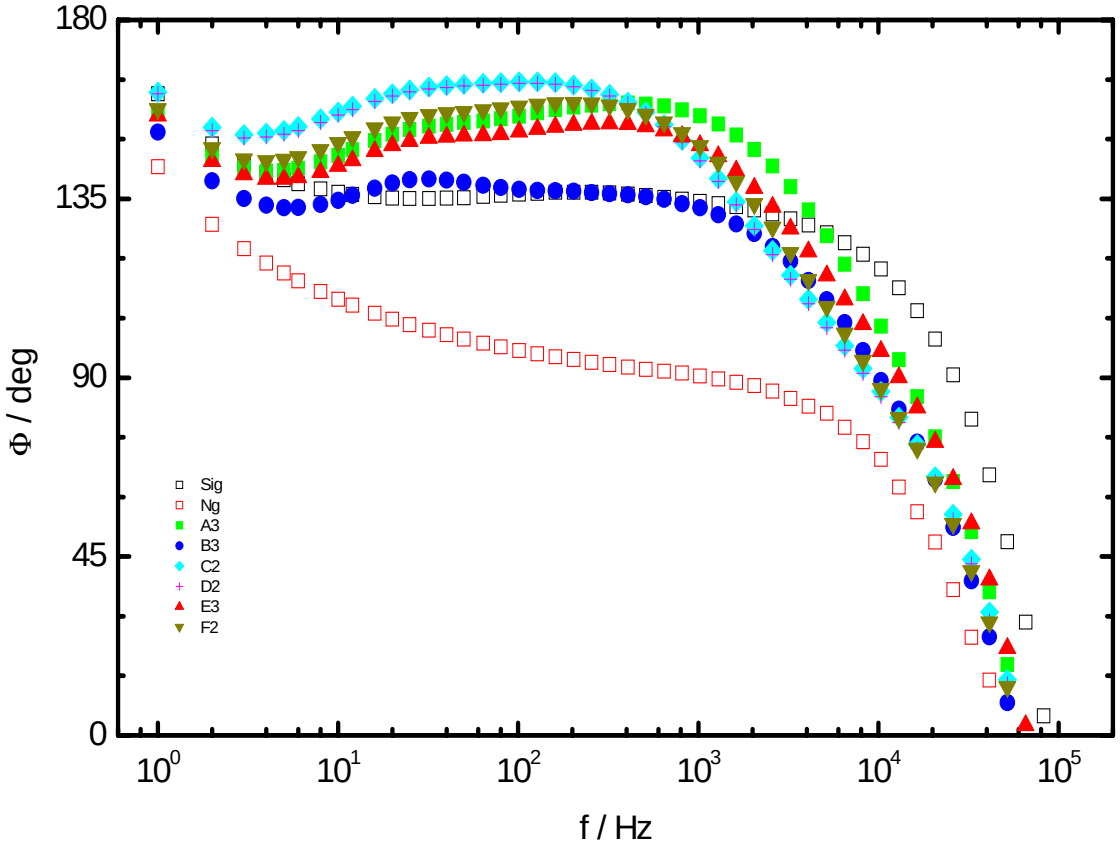

Figure 5. Modulated IR phases measured as a function of the heating modulation frequency for coated steel sheet test samples, in comparison with the reference signals measured for an opaque homogeneous sample of glassy carbon (Sigradur ◘) and a semi-transparent sample of neutral density glass (Schott NG1 ◘)

In the range of intermediate modulation frequencies, the modulated IR phases of all coated test samples, A(■), B(●), C(♦), D(+), E(▲), and F(▼) show values between 135° and 180°, and are thus found above the modulated IR phases of the opaque homogeneous glassy carbon reference sample. At larger modulation frequencies, corresponding to smaller penetration depths of the thermal waves, the modulated IR phases of the coated test samples are found between the phase values of the opaque reference samples and those of the semi-transparent reference sample. This means that the coatings of all test samples show effects of semi-transparency, which can be explained by the fact that the thermal diffusion length in this frequency range becomes comparable with the effective optical absorption length of the coating,

$$\mu_{th} = \sqrt{\alpha/(\pi f)} \approx ß^{-1} \quad (2)$$

In agreement with the modulated IR amplitudes, also the modulated IR phases of the samples C(♦) and D(+) are very close to each other (Compare Table 1). Additionally, the modulated IR phases of sample F(▼) show a behavior similar to the modulated IR phases of the sample A(■) and E(▲). Considering the general frequency behaviour of the measured modulated IR signals, both the amplitudes (Fig. 4) and the phases (Fig. 5), two groups of similar samples can be identified, namely the groups {C,D} and {A, E, F}, while the sample B(●) considerably deviates from these two groups (Compare Table 1).

3.1 Characterization of coated steel sheet samples based on calibrated measurements

In order to eliminate the frequency characteristics of the measurement device, the signals measured for the coated steel sheet samples are subsequently calibrated with the help of the signals measured for the opaque homogeneous reference sample of glassy carbon. For the further qualitative discussion and a possible quantitative interpretation, the amplitude and phase signals can be represented in the form

$$S_n^{-1}(f) = S_{ref}(f)/S_s(f) \quad (3)$$

$$\Phi_n(f) = \Phi_{ref}(f) - \Phi_s(f) \quad (4)$$

In equ. (3) and (4), $S_{ref}(f)$ and $S_s(f)$ are the modulated IR amplitudes measured for the reference and the coated steel sheet samples, and $\Phi_{ref}(f)$ und $\Phi_s(f)$ are the corresponding modulated IR phases.

The inverse calibrated signal amplitudes according to equ.(3) can additionally be normalized to the value of 1 at large penetration depths $x \propto \mu_{th} = \sqrt{\alpha/(\pi f)} \to \infty$, corresponding to small modulation frequencies $f \to 0$,

$$\frac{S_n^{-1}(f)}{S_n^{-1}(f \to 0)} = \frac{[S_{ref}(f)/S_s(f)]}{[S_{ref}(f \to 0)/S_s(f \to 0)]} \quad (5)$$

This additional normalization is a useful operation, since at small modulation frequencies and large penetration depths the thermal properties of the substrate material are measured which are equal for all measured coated steel sheet samples, and since in this form (Fig. 6) the coated steel sheet test samples can directly be compared with each other.

At higher modulation frequencies corresponding to smaller penetration depths (left hand side of Fig.6), the normalized inverse calibrated signals are influenced by the effective absorption constant ß, respectively by the effective absorption length $ß^{-1}$, which is comparable with (equ.2) or larger than or the thermal diffusion length. Samples with less transparent coatings, e.g. sample A (■), show a smaller negative slope in the range of small penetration depths than samples with more transparent coatings, e.g. sample D(+) and sample B(●). In addition, the range of the negative slope is shorter for less transparent samples, e.g. for sample A (■) a relative minimum is found at about $(f/\mathrm{Hz})^{-1/2} \approx 0.015$ whereas for sample D(+) and B(●) the relative minima are found between about $(f/\mathrm{Hz})^{-1/2} \approx 0.020$ and 0.025. At very high modulation frequencies, corresponding to values of $(f/\mathrm{Hz})^{-1/2} < 0.006$, the signals measured for sample B(●) are close to the noise limit and thus are not reliable (Fig. 6).

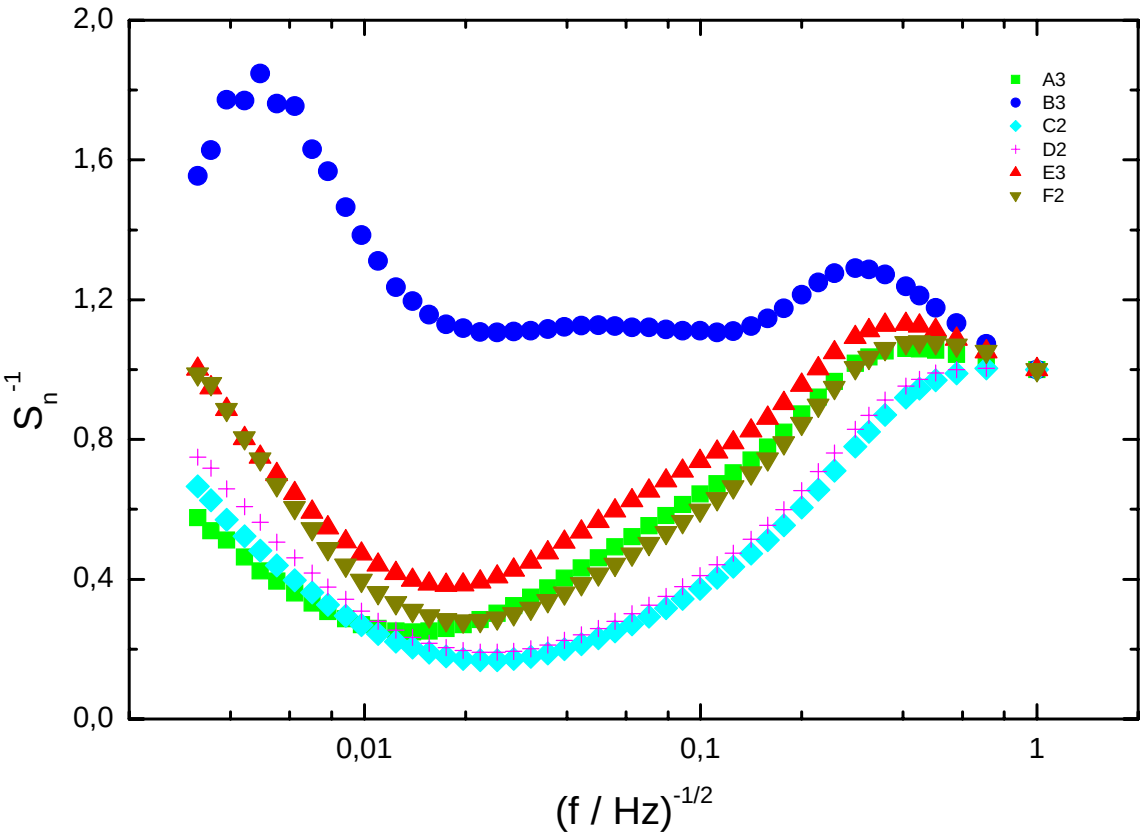

Figure 6. Inverse calibrated modulated IR amplitudes of the coated steel sheet test samples after additional normalization on the value of 1 at large penetration depths.

In the range of intermediate and lower modulation frequencies, corresponding to intermediate and larger penetration depths, $0.02 \leq (f/\mathrm{Hz})^{-1/2} \leq 0.4$, the increase of the normalized inverse calibrated IR amplitudes with the penetration depth is governed by the thermal properties of the layer structure.

In Figure 6 it can clearly be seen, that the two samples D(+) and C(♦) are thermally very similar and that they only differ in the limit of very high modulation frequencies, $f >$ 10 kHz, corresponding to very small penetration depths, where the coating of sample D is slightly more transparent.

The differences within the group of similar samples {A, E, F} are slightly larger. At intermediate and low modulation frequencies, corresponding to intermediate and large penetration depths, the two samples A (■) and F (▼) only show small differences (Fig. 6), whereas at high modulation frequencies, corresponding to small penetration depths, larger differences can be seen, pointing towards a larger transparency of the surface-near first layer of sample F(▼). The samples E(▲) and F(▼) show larger differences at intermediate and large penetration depths (right hand side of Fig. 6), which are related to a different layer thickness. At smaller penetration depth, on the other hand, the signals of these two samples are very close to each other (left hand side in Fig. 6), which means that similar transparency properties are measured close to the surface.

Sample B(●), which according to the measured amplitude and phase signals (Fig. 4 and 5) can not be attributed to one of the two sample groups, shows a behavior similar to that of the samples E(▲) and F(▼), when the inverse calibrated amplitudes are considered in the limit of small penetration depths, $(f/\mathrm{Hz})^{-1/2} < 0.01$, corresponding to high modulation frequencies. The slopes of the inverse calibrated amplitudes are similar, which means that close to the sample surfaces similar effects of semi-transparency are measured.

To distinguish between semi-transparency in the IR spectral range and in the visible spectral range, the inverse calibrated photoacoustic phases (Figure 7), which only depend on the thermal properties and the semi-transparency in the visible spectrum, are compared with the inverse calibrated modulated IR phases (Figure 8), which additionally depend on the semi-transparency in the IR spectral range.

In general, the inverse calibrated phases of opaque coatings are close to the *zero line* at high modulation frequencies, whereas for semi-transparent coatings, the inverse calibrated phases can exceed the *zero line* considerably. The inverse calibrated photoacoustic phases of all test samples exceed the *zero line* at higher modulation frequencies (Fig. 7), which means the coatings of all samples are semi-transparent in the visible spectrum: – According to Figure 7 sample A (■), with its inverse calibrated phases crossing the *zero line* at about $f_0 \approx 4.6$ kHz, is the less transparent sample. The samples C(♦), D(+), E(▲) and F(▼), with the inverse calibrated phases crossing the *zero line* at approximately the same modulation frequency, $f_0 \approx 1.6$ kHz, are more transparent, and sample B(●), for which the crossing point between inverse calibrated phases and *zero line* is already found at about $f_0 \approx 500$ Hz is the sample with the highest semi-transparency in the visible spectrum.

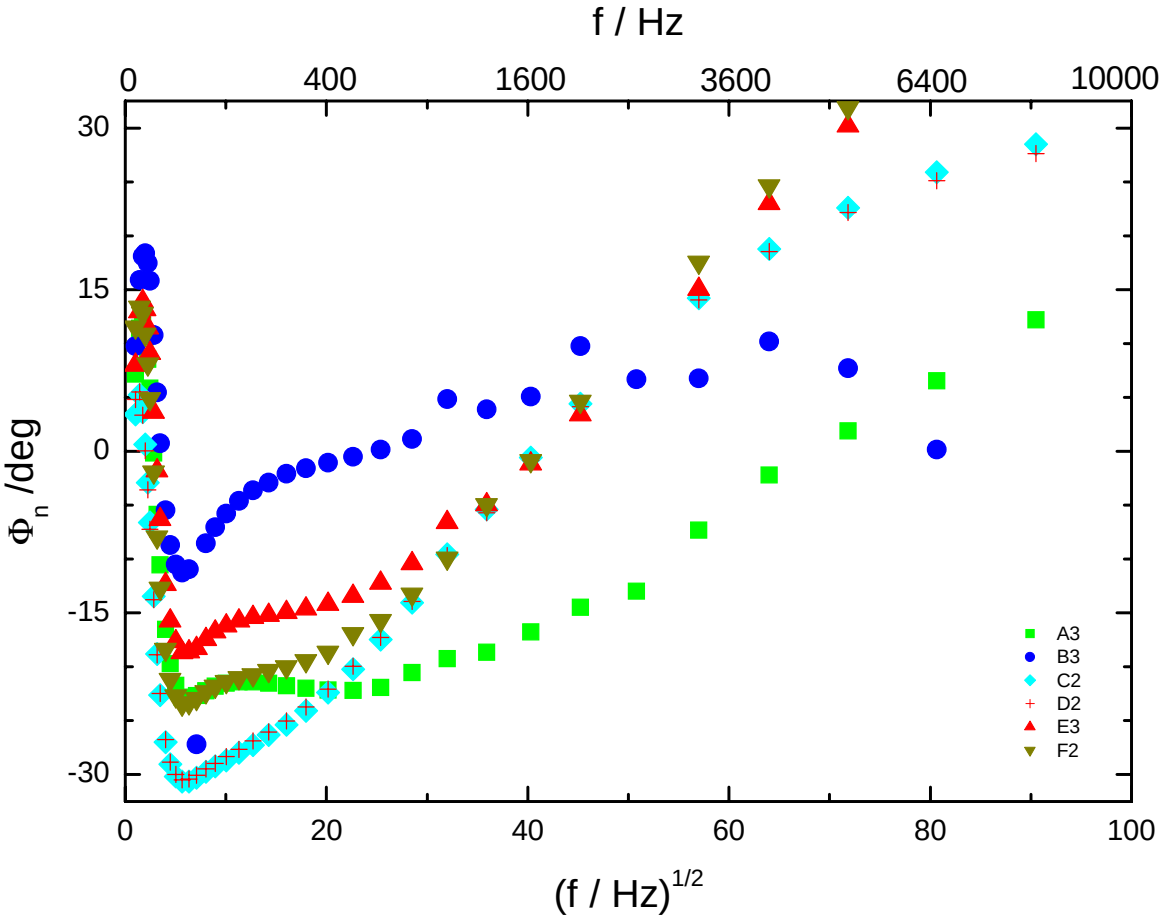

Figure 7. Inverse calibrated photoacoustic phases obtained for the coated steel sheet test samples

The effects of semi-transparency on the measured signal can be characterized by comparing the optical and/or IR-optical absorption lengths with the thermal diffusion length. Thus in two-layer systems consisting of coating and substrate the effects of semi-transparency are negligible [5], when the absorption lengths are small compared to the thermal diffusion length $\beta_{vis,IR}^{-1} << \mu_{th} = \sqrt{\alpha/(\pi f)}$ of the coating, and they become relevant, when the absorption lengths are comparable with $\beta_{vis,IR}^{-1} \approx \sqrt{\alpha/(\pi f)}$ or larger than the ther-

mal diffusion length. Here, the modulation frequency at the crossing point between inverse calibrated phases and *zero line* is used to characterize the optical absorption length,

$$[\beta_{vis}^{-1}]_A \approx 1/\sqrt{f_0} \approx 0.015 < [\beta_{vis}^{-1}]_{C,D,E,F} \approx 0.025 < [\beta_{vis}^{-1}]_B \approx 0.045 \quad (6)$$

Comparing coating B (without zinc particles) with coating A (containing zinc particles) its optical absorption length is larger by a factor of 3.

Comparing the inverse calibrated modulated IR phases (Fig. 8) with the inverse calibrated photoacoustic phases (Fig. 7), one can see that the phases measured for the various test samples by means of modulated radiometry can be better distinguished than the phases measured by photoacoustics. While the photoacoustic phases of the samples C, D, E and F had a common crossing point with the *zero line* at about f_0 = 1.6 kHz, the inverse calibrated modulated IR phases (Figure 8) show a considerable differentiation with $f_0 \approx 2.7$ kHz for sample E, $f_0 \approx 2.2$ kHz for sample F, $f_0 \approx 1.65$ kHz for samples C and D, pointing towards differences in the effective absorption lengths in the IR spectrum,

$$[\beta_{IR}^{-1}]_A \approx 1/\sqrt{f_0} \approx 0.014 < [\beta_{IR}^{-1}]_E \approx 0.019 < [\beta_{IR}^{-1}]_F \approx 0.021 < [\beta_{IR}^{-1}]_{C,D} \approx 0.0245 < [\beta_{IR}^{-1}]_B \approx 0.08 \quad (7)$$

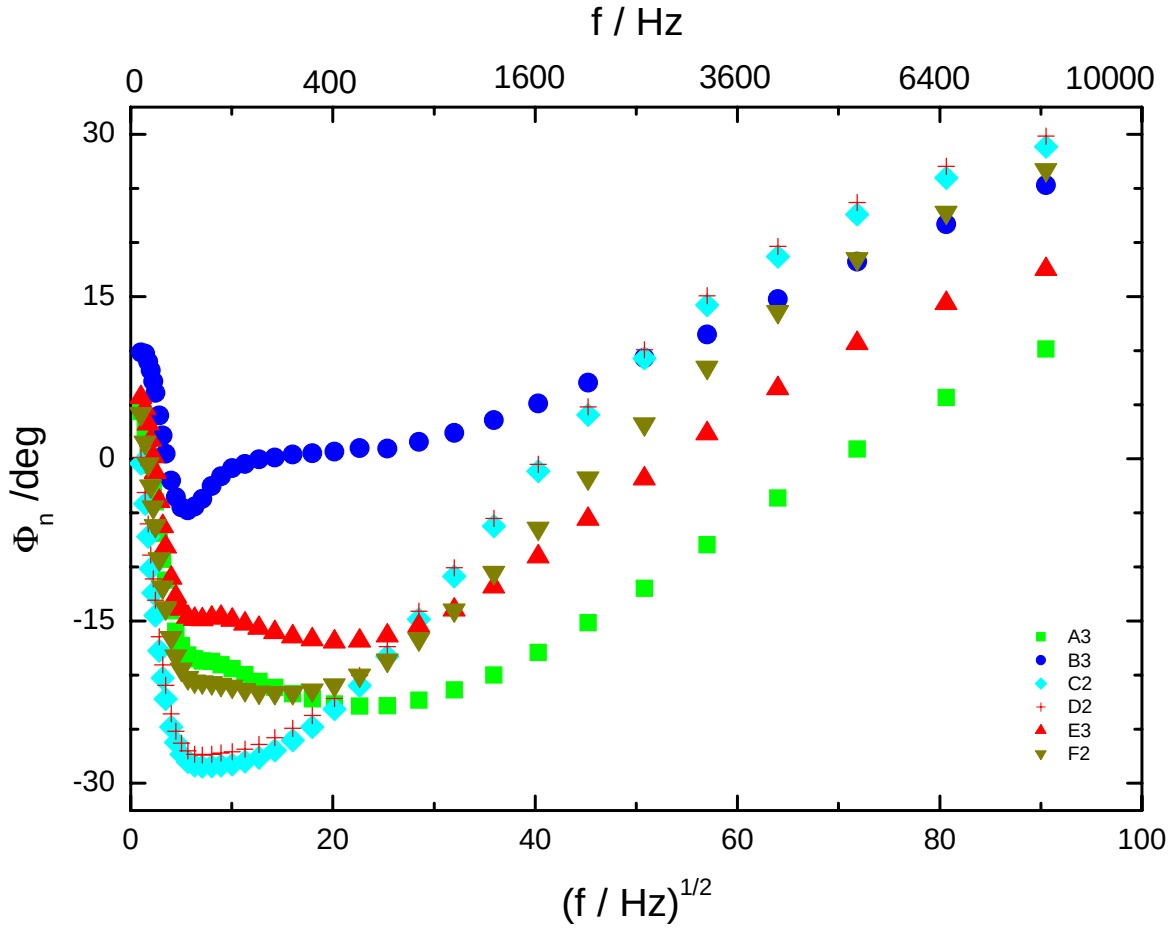

Figure 8. Inverse calibrated modulated IR phases obtained for the coated steel sheet test samples

This means that the various coatings with and without zinc particles can be characterized and distinguished according to their effective thermal and IR-optical properties:

- The different layer structures A, B, C, D, E and F show significant differences in the frequency behavior of the inverse calibrated modulated IR phases (Fig. 8). At low and intermediate modulation frequencies the samples can be distinguished and identified according to their relative phase minima $\{f_{min}, \Phi_{n\,min}\}$, namely the modulation frequencies and the values of the relative minima. According to ref. [5] the phase minimum value gives information on the ratio of the effusivity coating-to-substrate,

$$g_{sb} = e_s / e_b = \sqrt{(k\rho c)_s} / \sqrt{(k\rho c)_b} \qquad (8)$$

and the modulation frequency at the relative minimum gives information on the *thermal thickness* or thermal diffusion time of the coating,

$$\tau_s = d_s^2 / \alpha_s \qquad (9)$$

Here, the quantities k, ρ, and c represent the thermal conductivity, the mass density and the specific heat capacity, the index s refers to the coating and b to the substrate, and d_s and α_s are the thickness and the effective thermal diffusivity of the coating.

- The crossing point $f_0 = f(\Phi_n = 0)$ between the *zero line* and the inverse calibrated modulated IR phases and the phase offset at high modulation frequencies give information on the effective absorption length in the IR spectrum.

Once the sensitivity of modulated IR radiometry to semi-transparent coatings with and without zinc particles and to the distribution of the particles within the coating had been proven, measurements on real production samples with differing welding properties were undertaken.

4. Photothermal Discrimination under Industrial Conditions

The frequency-dependent measurements of coated steel sheet samples of good (GB) and bad (SB) welding properties have shown that the SB samples of bad welding properties can generally well be distinguished from the GB samples of good welding properties, by means of both the modulated IR amplitude and phase. In addition, among the GB samples two groups of samples have been identified which can be characterized according to their effective thermal properties. Among the SB samples four samples could be identified differing from the other SB samples with respect to a reduced substrate thickness.

Based on the experience gained so far, the following method seems to be appropriate to distinguish and to separate steel sheets of good and bad welding properties under industrial conditions: – separation according to the depth profiles of the inverse normalized modulated IR amplitudes, $S_{GB\,ref}/S_{sample}$, using a sample of good welding properties as reference for normalization (Figure 9).

At intermediate modulation frequencies and penetration depths, $0.015 < (f/\mathrm{Hz})^{-1/2} < 0.15$, two groups of GB samples of good welding properties can be identified in Figure 9, with the relative amplitudes in the range of

$$0.93 < S_{GBref}/S_{sample} < 1.1 \quad \text{and} \quad 1.15 < S_{GBref}/S_{sample} < 1.28 \qquad (10)$$

The relative amplitudes of the SB samples of bad welding properties are found, well separated, in the range of

$$1.4 < S_{GBref}/S_{sample} < 1.72 \qquad (11)$$

One of the samples of bad welding properties, (Δ 61436 A), which according to the thermal depth profile and to SEM has probably got a locally inhomogeneous coating is found at intermediate modulation frequencies in the range of the S_{GBref}/S_{sample} values of the GB samples of good welding properties. At high modulation frequencies, $(f/\mathrm{Hz})^{-1/2} < 0.01$,

corresponding to small penetration depths, however, this sample is well separated from the GB samples and is found in the range of S_{GBref}/S_{sample}-values of the samples of bad welding properties (Figure 9).

It is also interesting to see in Figure 9, that two samples of bad welding properties, { ▲ 15230 A, ▼ 15230 B }, which at intermediate modulation frequencies and penetration depths are found in the appropriate range, namely $1.4 < S_{GBref}/S_{sample} < 1.72$, can be found at high modulation frequencies and very small penetration depths in the range of the samples of good welding properties. Insight in this physical behavior is still missing.

For the discrimination and separation of coated steel sheets in an industrial coating process and the on-line control of the coating's quality, frequency-dependent measurements over a large interval of heating modulation frequencies, as presented in Figure 9, are not possible, since the required measurement time would be too large. Instead, measurements at two or three selected heating modulation frequency values are recommendable, where the quality of the coating can be evaluated with sufficient reliability.

For measurements at larger penetration depths, where the modulated IR signal gives information on the transition region between coating and steel substrate, according to Fig. 9 the range of

$$0.07 < (f/\mathrm{Hz})^{-1/2} < 0.1 \qquad \text{corresponding to} \qquad 100\ \mathrm{Hz} < f < 200\ \mathrm{Hz} \qquad (12)$$

would be appropriate, since the effects of a reduced thickness of the steel sheet substrate are not yet measurable.

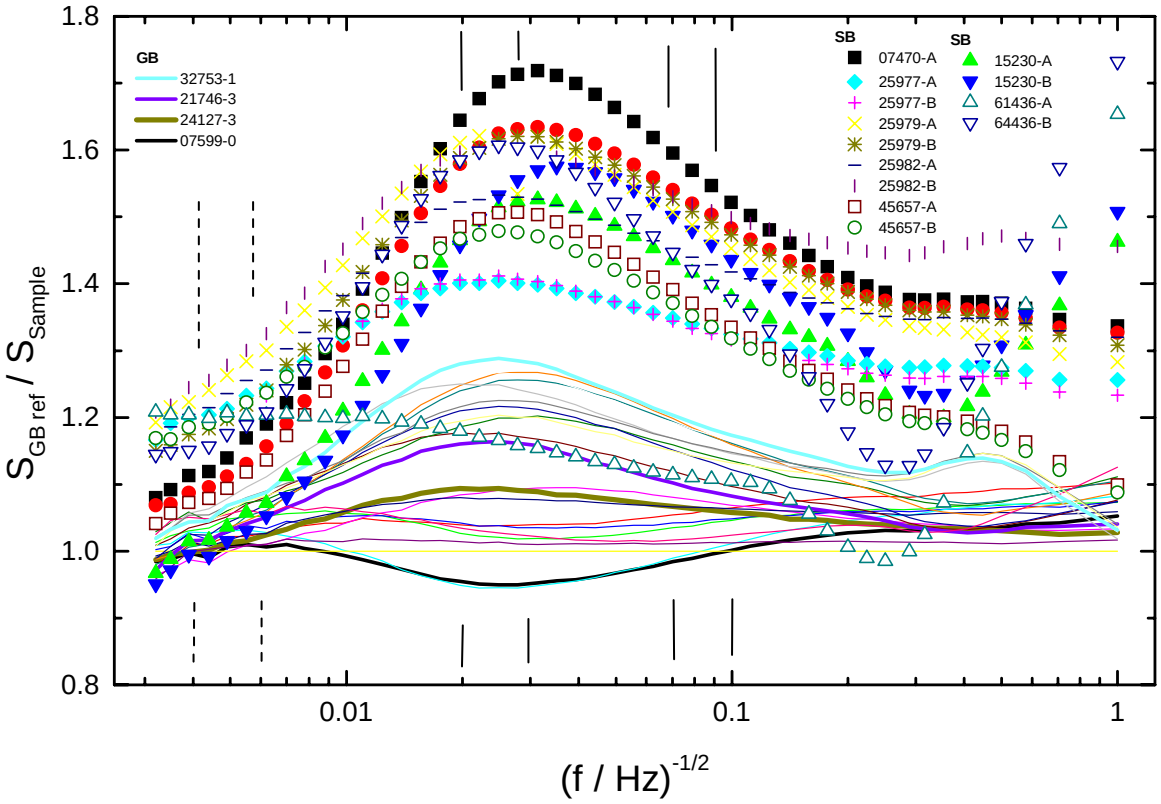

Figure 9. Inverse normalized modulated IR amplitudes S_{GBref}/S_{sample} versus the penetration depth of the thermal wave, using an arbitrary SB sample of good welding properties (GB 24127) as reference sample for normalization.

For the measurement at intermediate modulation frequencies and penetration depths, where according to Figure 9 the differences between the samples of good and bad welding properties are most pronounced, the range of

$$0.02 < (f\,/\mathrm{Hz})^{-1/2} < 0.04 \qquad \text{corresponding to} \qquad 625\ \mathrm{Hz} < f < 2.5\ \mathrm{kHz} \qquad (13)$$

would be appropriate.

In order to eliminate coated steel sheets of bad welding properties, such as sample 61436 A (Δ), which in the range of low and intermediate modulation frequencies fulfill the criteria for samples of good welding properties, measurements should also be done at very high modulation frequencies corresponding to small penetration depths

$$0.004 < (f\,/\mathrm{Hz})^{-1/2} < 0.006 \qquad \text{corresponding to} \qquad 28\ \mathrm{kHz} < f < 62\ \mathrm{kHz} \qquad (14)$$

which mainly give information on the transparency of the coatings, both in the visible and in the IR spectral range.

In a reliable and fast separation method, appropriate for the on-line quality control during the production process, a coated steel sheet sample fulfilling only one of the criteria of samples of bad welding properties, should already be excluded. Thus, first the measurement should be done at the very high modulation frequencies, corresponding to very small penetration depths (14). Subsequently the measurement should be done at the intermediate modulation frequencies and penetration depths (13), and only finally the measurement is done at comparatively smaller modulation frequencies, corresponding to the larger penetration depths (12).

5. Conclusions and Outlook

In photothermal tests relying on modulated IR radiometry and photoacoustic detection, it has been found that semi-transparent organic coatings on steel sheet samples with discrete distributions of zinc particles can well be distinguished, both by the measured thermal wave amplitudes and the phase lags. Additionally it has been found that – depending on the zinc particle distribution - the coatings exhibit different depth profiles of the effective thermal properties and different effects of semi-transparency, whereby effects optical and IR-optical semi-transparency can be distinguished.

In measurements of real production samples based on nondestructive and contactless modulated IR radiometry, it was possible for the first time to clearly identify and separate coated steel samples of good and bad welding properties empirically.

In order to apply this empirical procedure of identification and separation of coated steel sheets in industry further studies still have to be undertaken referring to the measurement process in general and to the coating process in special. For this purpose, an offline IR radiometry laboratory system, running parallel to production would be of great value. For the fast on-line quality control under industrial conditions, the required measurement time has to be optimized. This can be achieved by optimizing time constants and statistics of the lock-in process for such semi-transparent coatings. In addition the measuring system has to be adapted to the specific conditions of remote detection [4].

Apart from analysing more examples of coated steel sheet samples, to get a larger basis of experience for the empirical identification of good and bad weldability, the measured frequency-dependent depth profiles have to be interpreted quantitatively with respect to the effective thermal and IR-optical properties of the coatings. This is necessary for a physical and not purely empirical correlation between the photothermal measurements and the thermophysics of the welding process, considering heat generation and conductive and radiative heat transport in the semi-transparent coatings.

References:

[1] Autorenkollektiv (Voestalpine Stahl, Arcelor, Corus R&D, SZMF, TKS, DOC, VDEh, Opel, Daimler-Chrysler), "Status of corrosion protection primers for the automotive industry." SCT 2005, International Conference on Steels in Cars and Trucks, Wiesbaden, 05.-10.06.2005.

[2] C. Fritzsche, H. Beenken, I. Maronna, F. Onno, J. Szinyur, ”Schweißeignung von organisch dünn-film-beschichteten Feinblechen“, 2nd European Status Conference, “Precoated Materials in Carbody Manufacturing”, Bad Nauheim 2001, 91-98.

[3] J. Gibkes, J.L. Nzodoum Fotsing, K. Simon, B.K. Bein, J.Pelzl, “Calibration of Infrared Signals by the Photoacoustic Effect”, Invited contribution in Proc. DAGA 02, Ed. DAGA e.V., Oldenbourg Verlag, 2002.

[4] J. Bolte, J.H. Gu, B.K. Bein, “Background Fluctuation Limit of IR Detection of Thermal Waves at High Temperatures”, High Temp.- High Pressures 29, 567-580, 1997.

[5] J. L. Nzodoum Fotsing, J. Gibkes, J. Pelzl, and B. K. Bein, “Extremum method: Inverse solution of the two-layer thermal wave problem”, J. Appl.Phys. 98, 6 (2005) 063522-1-17.